HHS Public Access

Author manuscript

Med Nov Technol Devices. Author manuscript; available in PMC 2022 September 22.

Published in final edited form as:

Med Nov Technol Devices. 2022 September ; 15: . doi:10.1016/j.medntd.2022.100153.

Computational fluid dynamics analysis and experimental hemolytic performance of three clinical centrifugal blood pumps: Revolution, Rotaflow and CentriMag

Dong Han[a], **Joshua L. Leibowitz**[a], **Lu Han**[a,1], **Shigang Wang**[a], **Ge He**[a,2], **Bartley P. Griffith**[a], **Zhongjun J. Wu**[a,b,*]

[a]Department of Surgery, University of Maryland School of Medicine, Baltimore, MD, USA

[b]Fischell Department of Bioengineering, A. James Clark School of Engineering, University of Maryland, College Park, MD, USA

Abstract

Centrifugal blood pumps have become popular for adult extracorporeal membrane oxygenation (ECMO) due to their superior blood handling and reduced thrombosis risk featured by their secondary flow paths that avoid stagnant areas. However, the high rotational speed within a centrifugal blood pump can introduce high shear stress, causing a significant shear-induced hemolysis rate. The Revolution pump, the Rotaflow pump, and the CentriMag pump are three of the leading centrifugal blood pumps on the market. Although many experimental and computational studies have focused on evaluating the hydraulic and hemolytic performances of the Rotaflow and CentriMag pumps, there are few on the Revolution pump. Furthermore, a thorough direct comparison of these three pumps' flow characteristics and hemolysis is not available. In this study, we conducted a computational and experimental analysis to compare the hemolytic performances of the Revolution, Rotaflow, and CentriMag pumps operating under a clinically relevant condition, i.e., the blood flow rate of 5 L/min and pump pressure head of 350 mmHg, for adult ECMO support. *In silico* simulations were used to characterize the shear stress distributions and predict the hemolysis index, while *in vitro* blood loop studies experimentally determined hemolysis performance. Comparative simulation results and experimental data demonstrated that the CentriMag pump caused the lowest hemolysis while the Revolution pump generated the highest hemolysis.

*Corresponding author. Department of Surgery, University of Maryland School of Medicine, 10 South Pine Street, MSTF 436, Baltimore, MD, 21201, USA. zwu@som.umaryland.edu (Z.J. Wu).

[1]Current affiliation: Department of Cardiothoracic Surgery, Shanghai Children's Medical Center, Shanghai Jiao Tong University, Shanghai, China.

[2]Current affiliation: Shanghai Key Laboratory of Mechanics in Energy Engineering, School of Mechanics and Engineering Science, Shanghai University, Shanghai, China.

Author contribution

Dong Han: Data curation, Formal analysis, Investigation, Writing – original draft, Writing – review & editing. **Joshua L. Leibowitz**: Formal analysis, Writing – review & editing. **Lu Han**: Data curation, Writing – original draft. **Shigang Wang**: Investigation. **Ge He**: Data curation, Writing – original draft. **Bartley P. Griffith**: Funding acquisition. **Zhongjun J. Wu**: Conceptualization, Funding acquisition, Methodology, Resources, Writing – review & editing.

Declaration of competing interest

Z.J.W. and B.P.G. disclose financial interest in Abiomed/Breethe, Inc. and intellectual property for ECMO systems and blood pumps. All other authors declare that they have no conflict of interest in the subject matter or materials reported in this study.

Keywords

CFD; ECMO support; Centrifugal blood pumps; Hemolysis

1. Introduction

Blood pumps have been increasingly used in a broad range of clinical applications, including temporary and durable ventricular assist devices (VAD), extracorporeal membrane oxygenation (ECMO), and cardiopulmonary bypass (CPB) for cardiac surgery. Roller pumps and centrifugal pumps are the two basic types of blood pumps commonly used in extracorporeal life support (ECLS) [1-3]. In neonatal ECMO, roller pumps were preferred due to their small priming volume and reliable constant flow rate [4]. However, they may induce high outlet pressure levels, leading to the risk of connection disruption. In addition, the high shear force created at the leading edge of the roller can crush cellular blood components leading to hemolysis. By contrast, centrifugal pumps act through a spinning rotor to generate blood flow, thereby will not pump against high resistance and will avoid high pressures in the case of distal circuit occlusion. In the past decade, centrifugal pumps have been the predominant pump used for ECMO treatment in adults [5-7].

Centrifugal blood pumps have been widely used in adult CPB and particularly ECMO, where prolonged use (weeks to months) is often necessary [8]. Recent clinical practice also shifted from roller pumps to centrifugal pumps for pediatric ECMO by adjusting their operating flow rates and rotational speeds [9,10]. For example, CentriMag pumps have also been successfully used in pediatric patients requiring VAD and ECMO support [11,12]. Currently, the Revolution pump (LivaNova, London, UK), the Rotaflow pump (Getinge, Gothenburg, Sweden), and the CentriMag pump (Abbott, Chicago, IL, USA) are three of the leading centrifugal blood pumps on the market for ECMO and CPB applications. They are all magnetically driven by a similar platform (motor and controller console) and have wash-out holes in the middle of the impellers to maintain a continuous flow path. While these centrifugal blood pumps feature a secondary flow path design, which avoids flow stagnation to reduce the risk of thrombosis in the pumps [13,14], they can potentially still produce high shear stress regions due to the necessary high rotational speeds of their impellers [15]. With the increasing use of centrifugal blood pumps in ECMO patients, commonly reported complications associated with high shear stress include bleeding, stroke, and thromboembolic events [3,16-18].

Device-related high shear stress (above 10 Pa), or non-physiological shear stress (NPSS), is believed to damage blood cells leading to altered blood function that has adverse effects on patients [19-22]. Conventionally, the size of NPSS regions and the rate of red blood cell (RBC) damage (hemolysis level) are two primary metrics for evaluating the hemocompatibility of different blood pumps [14,23]. Minimizing the risk of blood damage (i.e., hemolysis) with these pumps is critical, especially for the long-term ECMO support. In the literature, many *in vitro* experiments (hemolysis tests) and computational fluid dynamics (CFD) simulations have focused on evaluating the hemolytic behavior of the Rotaflow and CentriMag pumps [24-27]. However, few studies have been performed on the Revolution

pump. In addition, a thorough direct comparison of these three pumps in terms of their shear stress distribution and *ex-vivo* hemolysis under clinically relevant conditions is still not available. Therefore, in this paper, we used both computational and experimental methods to compare the hemolytic performance of the Revolution pump, the Rotaflow pump, and the CentriMag pump. The experimental and simulation data provide insight on centrifugal pump use for ECMO support or CPB under a typical clinical flowrate and pressure head. The dynamic characteristics and hemolytic performances of these pumps may also be used as references for the future design of centrifugal pumps with a better biocompatibility.

2. Pump characteristics

The three-dimensional (3D) structures of the (a) Revolution, (b) Rotaflow, and (c) CentriMag pumps are shown in Fig. 1. All the pumps have a magnetically driven impeller with different designs. The Revolution pump is an unshrouded impeller pump that employs a magnetically stabilized impeller molded onto a steel shaft rotating on two bearings at each end. The CentriMag pump impeller is unshrouded and uses bearingless magnetic levitation that stabilizes the impeller through electromagnetic forces. In contrast to the Revolution and CentriMag pumps, the Rotaflow pump is a shrouded impeller pump that features a peg-top, one-point, sapphire bearing on the bottom designed to reduce friction. The primary flow path is from the inlet to the tangential outlet through the impeller blade passage, as illustrated in Fig. 1. The secondary flow path is located in the small gaps between the rotor and stationary housing, as schematically shown in Fig. 2, exemplified with a schematic view of the CentriMag pump.

The Revolution pump weights 94.5 g with a priming volume of 57 mL and has an operational rotating speed of up to 3,500 rpm and a flow rate up to 8 L/min. The Rotaflow pump weighs 61.3 g with a priming volume of 32 mL and can provide a maximum blood flow rate of 9.9 L/min and a rotating speed up to 5,000 rpm. The CentriMag pump weighs 67.3 g with a priming volume of 31 mL. It can deliver a maximum blood flow rate of 9.9 L/min and a maximum rotating speed of 5,500 rpm. The general features of the three pumps are summarized in Table 1.

3. CFD modeling approach

The 3D models of these pumps (Fig. 1) were either obtained from available computer-aided drawing (CAD) files or measured from actual device components with a reverse engineering procedure [28]. The fluid domains were extracted from the enclosed spaces between the pump housings and impellers. A commercial CFD package (Fluent 19.2, ANSYS, Inc, Canonsburg, PA) employing finite volume methods was utilized for the numerical simulations of these three pumps. The field variables, i.e., fluid velocity and pressure, were obtained by solving the governing (Navier-Stokes) equations of the fluid flow,

$$\rho[\partial \boldsymbol{u} \;/\; \partial t + (\boldsymbol{u} \cdot \nabla)\boldsymbol{u}] = \mu \nabla^2 u - \nabla p + \rho \boldsymbol{g} \tag{1}$$

where $\boldsymbol{u}$ is the velocity field of the fluid, t is the time, μ is the dynamic viscosity, ρ is the density, p is the pressure, and $\boldsymbol{g}$ is the external body force, such as gravity. Blood was

assumed as a homogeneous incompressible Newtonian fluid ($u_{i,i} = 0$) with a constant density of 1,050 kg/m^3 and viscosity of 0.0035 kg/m•s. The Semi-Implicit Method for Pressure Linked Equations (SIMPLE) pressure-velocity coupling scheme was used to solve the fluid governing equations with second-order accuracy and the Menter's Shear Stress Transport (SST) k-ω turbulence model was implemented in the numerical scheme. The pump impeller rotation was modeled using the multiple reference frame (MRF) approach. A constant mass flow rate of 0.0875 kg/min (i.e., 5 L/min) was prescribed at the inlet, and a zero-pressure condition was set for the outlet. Rigid and stationary walls were assumed to be nonslip. To mimic the clinical operating condition of the blood pumps, we controlled the pump pressure head (pressure difference between inlet and outlet) at 350 mmHg for all the pumps by adjusting the impeller's rotating speed, which resulted in 2,500 rpm, 3,600 rpm, and 4,000 rpm for the Revolution, Rotaflow and CertriMag pumps, respectively.

Both structured and unstructured elements were used for the meshing. Before the final CFD simulations, a mesh sensitivity study (also known as a mesh independence study) was performed following the process as described previously in modeling other centrifugal blood pumps [24,29]. The meshing processes yielded total element numbers of 13.4, 9.4, and 7.3 million for the Revolution, Rotaflow, and CentriMag pumps, respectively. Simulations were considered convergent when the following criteria were met: 1) all monitored residuals were smaller than 10^{-3}; 2) the outlet pressure reached a steady level; 3) the relative difference in the flow rate between the inlet and outlet was less than 5%. Wall shear stress (WSS) distributions, scalar shear stress (SSS) fields, and hemolysis indices were calculated from the convergent flow fields after simulations.

3.1. Shear stress and hemolysis index

NPSS is believed to damage RBCs leading to hemolysis which creates hemoglobinemia. Therefore, blood pumps with larger areas and volumes of NPSS distributions are more likely to have a higher average hemolysis level. To compare the hemolytic performances between these pumps, we first calculated WSS distributions on both impeller and housing surfaces and SSS distribution in the fluid domain around the impeller. SSS is defined as von-Mises-like stress [30],

$$\tau = \left[\frac{1}{6}\sum(\tau_{ii} - \tau_{jj})^2 + \frac{1}{2}\sum\tau_{ij}^2\right]^{1/2} \quad (2)$$

where τ_{ij} the shear stress tensor with $i \neq j$ rule applied in the above equation. Then the hemolysis index (HI), which quantitates the pumps' hemolysis potential, was obtained based on the conventional power-law hemolysis model,

$$HI(\%) = C\tau^{\alpha}t^{\beta} \quad (3)$$

where $C = 1.228 \times 10^{-5}$, $\alpha = 1.9918$ and $\beta = 0.6606$ for ovine blood [31]. HI represents the percentage change in plasma-free hemoglobin (PFH) relative to the total hemoglobin [32], which was measured at the pump outlet from the CFD simulation results by the Eulerian approach as detailed in Zhang et al. [14].

4. In vitro circulating flow loop

To examine the hemolytic performance of the three pumps, we used a small volume (500 mL) circulatory flow loop filled with fresh ovine blood, illustrated in Fig. 3. The tests were performed in compliance with the protocol for assessing hemolysis in continuous flow blood as recommended by the American Society of Testing and Materials (ASTM F1841-19) [33]. For all hemolysis tests, the blood flowrate was set in the range of 5.0 ± 0.2 L/min, and the pump pressure head was adjusted to be 350 ± 20 mmHg. The blood temperature was maintained at 37 ± 1 °C by immersing the blood reservoir in a warm water bath. The pump inlet and outlet pressures were measured by a calibrated piezoelectric pressure transducer (model 1502B01EZ5V20 GPSI, PCB Piezotronics, Inc, Depew, NY), and Transonic T410 flow meter (Transonic Systems, Ithaca, NY) and ultrasonic flow probe (model 9PXL, Transonic Systems, Ithaca, NY) were used to measure the volumetric blood flow rates.

The loop experiment for each device was repeated five times (n = 5) with fresh ovine blood collected through venipuncture from Lampire (Lampire Biological Laboratories, PA, USA). Blood collection containers were filled with heparin with a pre-calculated concentration of 10 U/mL blood to prevent blood from coagulation. Collected blood was then filtered with transfusion filters (PALL Biomedical, Fajardo, Puerto Rico) to remove any blood clots. Phosphate-buffered saline (PBS) (Quality Biological, Gaithersburg, MD, USA) was used to condition the filtered blood with a maintained hematocrit level of 30 ± 2%. The blood pH level was maintained at 7.4 ± 0.1 during the experiment by adding bicarbonate solution, and the total plasma protein was adjusted to be above 5.0 g/dL.

Finally, 500 mL pre-processed blood was then filled into each circulation loop. A baseline sample was collected from each loop immediately before the circulation, and blood samples were collected hourly for up to 6 h during the loop circulation. The plasma was obtained by centrifugation and measured for the PFH value described by Berk et al. [34]. The normalized index of hemolysis (NIH) was calculated following the equation from ASTM F1841-19,

$$NIH(\text{g / 100L}) = \Delta freeHb \times V \times \frac{100 - Ht}{100} \times \frac{1}{Q \times T} \quad (4)$$

where $\Delta freeHb$ is the increase of plasma-free hemoglobin concentration (g/L) over the sampling time interval T. V is the circuit volume. Q is flow rate. Ht is hematocrit.

5. Results

5.1. Flow feature and CFD predicted HI

The CFD solved streamlines and fluid velocity fields for each centrifugal pump are shown in Fig. 4. Blood entering from the inlet is accelerated by centrifugal force, moving radially along the impeller blade and reaching the maximum velocity on the tips of the impeller to enter the peripheral volute and then exit from the outlet. This flow path is also known as the primary flow path, which propels the most blood volume out of the pump chamber. The secondary flow path exists in the gap between the rotating impeller (hub and tip) and the stationary pump housing. Blood is driven in this path by the higher pressure near the

periphery of the hub and merges with the primary flow path in the central opening of the impeller. Another secondary flow path also exits in the flow domain between the top housing wall and the shroud surface for the Rotaflow pump.

Centrifugal pumps may generate high NPSS up to ~500 Pa under common clinical ECMO operating conditions due to the high rotation speed of their impellers [23,35,36]. The calculated WSS distributions on the impellers and housings of the Revolution, Rotaflow, and CentriMag pumps are displayed in Fig. 5. To quantitatively compare the worst blood damage impacted by the high level of WSS, we summed the higher WSS regions (WSS >200 Pa) areas on each pump's impeller and housing. The calculated areas of the impeller/housing surfaces with WSS higher than 200 Pa for the Revolution, Rotaflow, and CentriMag blood pumps are 120.4 mm^2/4,348.7 mm^2, 898.5 mm^2/2,064.8 mm^2, and 357.1 mm^2/3, 141.3 mm^2, respectively. The SSS distributions on a vertical midplane and a horizontal plane across the impeller blades of the three pumps are displayed in Fig. 6 (a). High SSS exists at either the impeller blade edges or the primary/secondary narrow flow channels. Fig. 6 (b) illustrates the regions with SSS higher than 200 Pa (colored in red) within the three pumps. The total volumes of these higher SSS regions for the Revolution, Rotaflow, and CentriMag pumps are 53.4 mm^3, 41.4 mm^3, and 43.2 mm^3, respectively.

Shear stress below 10 Pa is referred to as physiological shear stress (PSS), a level of shear stress that RBCs tolerate with minimal damage. Conversely, NPSS between 10 Pa and 100 Pa is believed to stretch RBCs, likely reversibly deforming their shape and extending the nano-pores on the RBC membrane surface, resulting in hemoglobin leakage [37,38]. In addition, NPSS higher than 100 Pa may irreversibly rupture RBCs, leading to the release of hemoglobin into plasma, causing severe hemolysis [39]. Therefore, we calculated the total WSS area and SSS volume of these three different shear stress ranges for each pump based on this concern, and the results are compared in Fig. 7. The CentriMag pump had the smallest area with WSS between 10 and 100 Pa and higher than 100 Pa, while the Revolution pump had the largest area with WSS between 10 and 100 Pa and a comparable area with WSS higher than 100 Pa to the Rotaflow pump. In terms of the SSS, the CentriMag pump had the smallest volumes with SSS between 10 and 100 Pa and higher than 100 Pa. The Revolution pump had the largest volumes with SSS between 10 and 100 Pa and higher than 100 Pa. The CFD predicted HI for the three pumps is shown in Fig. 8. The Revolution has the largest HI (1.59×10^{-4}) compared with the Rotaflow (1.48×10^{-4}) and the CentriMag (1.39×10^{-4}).

5.2. Hemolysis measurement

Fig. 9 shows the mean PFH concentration values of the baseline blood sample and the hourly collected blood samples from the circulating loops with the Revolution, the Rotaflow, and the CentriMag, and the NIH values for the three devices. The PFH concentrations of the blood samples at baseline in all devices were initially very similar and increased with the circulation time. The Revolution pump has the highest rate of increase in PFH, which was followed by the Rotaflow and then CentriMag. These results appear to be consistent with the calculated HI from CFD modeling. The average NIH value was 0.0287 ± 0.0041 g/100 L for

the Revolution pump, 0.0235 ± 0.0041 g/100 L for the Rotaflow, and 0.0152 ± 0.0019 g/100 L for the CentriMag.

6. Discussion

The flow dynamic and hemolytic performances of three commercially available centrifugal blood pumps (Revolution, Rotaflow, and CentriMag) under a clinically relevant operating condition were computationally and experimentally studied. Computational studies were conducted using Ansys/Fluent CFD simulations, and *in vitro* hemolysis experiments were performed in circulatory flow circuits filled with fresh ovine blood. The shear stress field, CFD predicted HI, and experimentally measured hemolysis were analyzed and compared between the three pumps. It should be noted that although they have a similar trend among these pumps in terms of hemolysis, CFD predicted HI is much smaller than the experimentally measured NIH. This is because CFD simulation can only evaluate hemolysis on one passage blood through the pump, while experiment measured NIH hourly that blood passed through the pump many times.

For the CFD field analysis, the comparisons were preliminary focused on WSS and volumetric SSS. The locations of the higher SSS (>200 Pa) distributions correlated with the locations of higher WSS (>200 Pa), as illustrated in Figs. 5 and 6. The un-shrouded Revolution and CentriMag pumps had similar patterns of WSS and SSS distributions, with higher level shear stress (>200 Pa) located at the near peripheral region of the top housing and blades' trailing edge. For the Rotaflow pump with a shrouded impeller, higher shear stress was also observed near the inner annular surface of its impeller shroud. It was observed that the size of higher WSS area (>200 Pa) on the housing, for all the pumps in Fig. 5, was larger than on the impeller. This is because the impeller is moving with the blood, whereas the housing is stationary, creating a significant fluid velocity difference near the wall that causes high WSS. The volumes of higher SSS (>200 Pa) of these pumps was quite similar, with the Revolution pump having the largest volume of 53.4 mm^2 and the Rotaflow pump having the smallest volume of 41.4 mm^3.

The Revolution pump had the smallest area of higher WSS surface on impeller, which was mainly located on the trailing edges of the blade tips, as shown in Fig. 5 (a). Like the un-shrouded Revolution pump, the impeller of the CentriMag pump also had a similarly large size of higher WSS distribution on the blades' trailing edges. Since the Revolution pump was larger in size, it required a slower rotational speed (2,500 rpm) than the CentriMag pump (4,000 rpm) to deliver the same amount of blood volume (5 L/min) from the inlet. This slower operating speed avoided sudden changes of the velocity field (illustrated in Fig. 4 (b)) along the blade, thus has a smaller area of higher WSS surface. Since the housing is stationary relative to blood flow, the larger size of the Revolution pump could result in a larger area of higher WSS on housing than the CentriMag pump. By contrast, the Rotaflow pump had the greatest area of higher WSS on the impeller but the smallest area of higher WSS on the housing among the three pumps. This resulted from the Rotaflow shroud design that prevented the blood flow delivered by the impeller from having the direct contact with the non-moving top housing which decreased the size of higher WSS surface on the top housing but at the cost of increased higher WSS surface area on the impeller. The shroud

design in centrifugal pumps can be critical to improve hemolytic performance as it shifts the high WSS from top housing to impeller. This may be even further optimized to achieve a better hemolytic performance. For example, a newly developed Breethe pump (Breethe, Inc, Baltimore, MD) with a compromised size of shroud showed a superior hemolysis to the CentriMag and Rotaflow pumps [15].

Although the CentriMag pump did not have the smallest area of higher WSS (housing and impeller) or volume of higher SSS, it had the smallest CFD predicted HI. When we calculated the WSS and SSS sizes in terms of the three different levels (i.e., <10 Pa, 10–100 Pa and >100 Pa), the CentriMag pump has a significantly large area of physiological WSS (<10 Pa) despite having the lowest priming volume (Fig. 7 (a)). CentriMag also has the smallest area and volume of NPSS (WSS and SSS), as shown in Fig. 7. Therefore, the CentriMag pump had the best computationally predicted hemolytic performance, consistent with the CFD predicted HI (Fig. 8) and experimental PFH/NIH values (Fig. 9). Although higher WSS and SSS regions indicated the locations that contribute to the worst blood damage, the hemolytic performance of different pumps was more likely related to the size of NPSS.

The Revolution pump had the worst hemolytic performance based on the CFD predicted HI and experimentally measured NIH. It also had the largest area of higher WSS surfaces (housing plus impeller), volume of higher SSS region and size of NPSS. This may be explained by the Revolution pump's large priming volume, which caused a longer blood exposure time and a larger area/volume of NPSS within the pump, leading to increased hemolysis. Although the Rotaflow pump had a similar priming volume and higher SSS volume to the CentriMag pump, it had a worse hemolytic performance than the CentriMag pump computationally and experimentally. This is best explained by the bearingless magnetically levitated impeller design of the CentriMag pump which likely reduced blood damage.

Other studies of the CentriMag and Rotaflow pumps using experimental and computational approaches can be found in the literature. Some concluded contradicting results, showing reduced hemolysis with the Rotaflow pump instead of the CentriMag pump [25], which may be attributed to different operating conditions and different blood species [15]. Our study used a clinically relevant condition for adult ECMO support in the simulation and experiment as centrifugal pumps have become the standard practice in most ECMO circuits. The careful selection of these centrifugal pumps for ECMO or CPB use also includes the cost, pump safety and reliability, and ease of set-up and use [40]. Centrifugal pumps can generate heat, especially when driven at high rotational speeds, changing blood temperature and consequently affect the gas exchange performance of oxygenators used in ECMO circuits. However, the pump heat generation was neglected in this study. In addition, the device-induced platelet activation and platelet receptors shedding [41-43], which is believed to be associated with thrombus formation and bleeding, is not measured in the current study.

7. Conclusion

The hemolytic performances of the Revolution, Rotaflow, and CentriMag pumps were computationally and experimentally studied with CFD analysis and *in-vitro* blood flow circuits under clinically relevant conditions for adult ECMO support. The CFD analysis showed that the CentriMag pump had the smallest areas and volumes of non-physiological WSS and SSS, and the smallest CFD predicted HI. It also had the smallest experimentally determined NIH compared to the Revolution and Rotaflow pumps. Additionally, blood samples from the CentriMag pump circular blood loop continuously had the lowest PFH concentrations during the 6-h study. Thus, our computational and experimental results demonstrated that the CentriMag pump had the best hemolytic performance compared with the Rotaflow and Revolution pumps.

Funding sources

The author(s) disclosed receipt of the following financial support for the research, authorship, and/or publication of this article: This work was funded by National Institutes of Health (Grant Numbers: R01HL118372, R01HL124170, R01HL131750, and R01HL141817).

This publication was made possible by the University of Maryland Baltimore Institute for Clinical and Translational Research (ICTR) which is funded in part by Grant Number TL1 TR003100 from the National Center for Advancing Translational Sciences (NCATS) a component of the National Institutes of Health (NIH), and NIH Roadmap for Medical Research. Its contents are solely the responsibility of the authors and do not necessarily represent the official view of the University of Maryland Baltimore ICTR, NCATS or NIH.

References

[1]. O'Brien C, Monteagudo J, Schad C, Cheung E, Middlesworth W. Centrifugal pumps and hemolysis in pediatric extracorporeal membrane oxygenation (ECMO) patients: an analysis of Extracorporeal Life Support Organization (ELSO) registry data. J Pediatr Surg 2017;52(6):975–8. 10.1016/j.jpedsurg.2017.03.022. [PubMed: 28359588]

[2]. O'Halloran CP, Thiagarajan RR, Yarlagadda VV, Barbaro RP, Nasr VG, Rycus P, et al. Outcomes of infants supported with extracorporeal membrane oxygenation using centrifugal versus roller pumps: an analysis from the ELSO registry. Pediatr Crit Care Med 2019;20(12):1177. https://www.ncbi.nlm.nih.gov/pmc/articles/PMC7175473/. [PubMed: 31567621]

[3]. Halaweish I, Cole A, Cooley E, Lynch WR, Haft JW. Roller and centrifugal pumps: a retrospective comparison of bleeding complications in extracorporeal membrane oxygenation. Am Soc Artif Intern Organs J 2015;61(5):496–501.

[4]. Lawson S, Ellis C, Butler K, McRobb C, Mejak B. Neonatal extracorporeal membrane oxygenation devices, techniques and team roles: 2011 survey results of the United States' Extracorporeal Life Support Organization centers. J Extra Corpor Technol 2011;43(4):236. https://www.ncbi.nlm.nih.gov/pmc/articles/PMC4557427/. [PubMed: 22416604]

[5]. Riley JB, Scott PD, Schears GJ. Update on safety equipment for extracorporeal life support (ECLS) circuits. In: Semin Cardiothorac Vasc Anesth, vol. 13. Los Angeles, CA: SAGE Publications Sage CA; 2009. p. 138–45. 10.1177/1089253209347895. [PubMed: 19720681]

[6]. Gadepalli SK, Hirschl RB. Extracorporeal life support: updates and controversies. Semin Pediatr Surg 2015;24:8–11. 10.1053/j.sempedsurg.2014.11.002. Elsevier. [PubMed: 25639803]

[7]. Han D, Shah A, Awad MA, Wu ZJ, Griffith BP. Development of an ambulatory extracorporeal membrane oxygenation system: from concept to clinical use. Appl Eng Sci 2022:100093. 10.1016/j.apples.2022.100093.

[8]. Alwardt CM, Wilson DS, Alore ML, Lanza LA, DeValeria PA, Pajaro OE. Performance and safety of an integrated portable extracorporeal life support system for adults. J Extra Corpor Technol 2015;47(1):38. https://www.ncbi.nlm.nih.gov/pmc/articles/PMC4566819/. [PubMed: 26390678]

[9]. Qiu F, Talor J, Zahn J, Pauliks L, Kunselman AR, Palanzo D, et al. Translational research in pediatric extracorporeal life support systems and cardiopulmonary bypass procedures: 2011 update. World J Pediatr Congenit Heart Surg 2011;2(3):476–81. 10.1177/2150135111402226. [PubMed: 23804000]

[10]. Clark JB, Guan Y, McCoach R, Kunselman AR, Myers JL, Ündar A. An investigational study of minimum rotational pump speed to avoid retrograde flow in three centrifugal blood pumps in a pediatric extracorporeal life support model. Perfusion 2011;26(3):185–90. 10.1177/0267659110394712. [PubMed: 21227983]

[11]. Maat AP, van Thiel RJ, Dalinghaus M, Bogers AJ. Connecting the Centrimag Levitronix pump to Berlin Heart Excor cannulae; a new approach to bridge to bridge. J Heart Lung Transplant 2008;27(1):112–5. 10.1016/j.healun.2007.10.010. [PubMed: 18187096]

[12]. Conway J, Al-Aklabi M, Granoski D, Islam S, Ryerson L, Anand V, et al. Supporting pediatric patients with short-term continuous-flow devices. J Heart Lung Transplant 2016;35(5):603–9. 10.1016/j.healun.2016.01.1224. [PubMed: 27009672]

[13]. Gregory S, Stevens M, Fraser JF. Mechanical circulatory and respiratory support. first ed. Academic Press; 2017.

[14]. Zhang J, Chen Z, Griffith BP, Wu ZJ. Computational characterization of flow and blood damage potential of the new maglev CH-VAD pump versus the HVAD and HeartMate II pumps. Int J Artif Organs 2020;43(10):653–62. 10.1177/0391398820903734. [PubMed: 32043405]

[15]. He G, Zhang J, Shah A, Berk ZB, Han L, Dong H, et al. Flow characteristics and hemolytic performance of the new Breethe centrifugal blood pump in comparison with the CentriMag and Rotaflow pumps. Int J Artif Organs 2021;44(11):829–37. 10.1177/03913988211041635. [PubMed: 34494469]

[16]. Erdem Ö, Kuiper JW, Houmes RJ, van Ommen CH, van Rosmalen J, Tibboel D, et al. Coagulation complications after conversion from roller to centrifugal pump in neonatal and pediatric extracorporeal membrane oxygenation. J Pediatr Surg 2021;56(8):1378–85. 10.1016/j.jpedsurg.2020.11.018. [PubMed: 33279215]

[17]. MacLaren G, Combes A, Bartlett RH. Contemporary extracorporeal membrane oxygenation for adult respiratory failure: life support in the new era. Intensive Care Med 2012;38(2):210–20. 10.1007/s00134-011-2439-2. [PubMed: 22147116]

[18]. Bemtgen X, Zotzmann V, Benk C, Rilinger J, Steiner K, Asmussen A, et al. Thrombotic circuit complications during venovenous extracorporeal membrane oxygenation in COVID-19. J Thromb Thrombolysis 2021;51(2):301–7. 10.1007/s11239-020-02217-1. [PubMed: 32653986]

[19]. Chen Z, Sun A, Wang H, Fan Y, Deng X. Non-physiological shear stress-induced blood damage in ventricular assist device. Med Novel Technol Devices 2019;3:100024. 10.1016/j.medntd.2019.100024.

[20]. Nevaril CG, Lynch EG, Alfrey CP, Hellums JD. Erythrocyte damage and destruction induced by shearing stress. J Lab Clin Med 1968;71(5):784–90. https://pubmed.ncbi.nlm.nih.gov/5647682/. [PubMed: 5647682]

[21]. Leverett L, Hellums J, Alfrey C, Lynch E. Red blood cell damage by shear stress. Biophys J 1972;12(3):257–73. 10.1016/S0006-3495(72)86085-5. [PubMed: 5016112]

[22]. Giersiepen M, Wurzinger L, Opitz R, Reul H. Estimation of shear stress-related blood damage in heart valve prostheses-in vitro comparison of 25 aortic valves. Int J Artif Organs 1990;13(5):300–6. 10.1177/039139889001300507. [PubMed: 2365485]

[23]. Fraser KH, Zhang T, Taskin ME, Griffith BP, Wu ZJ. A quantitative comparison of mechanical blood damage parameters in rotary ventricular assist devices: shear stress, exposure time and hemolysis index. J Biomech Eng 2012;134(8):081002. 10.1115/1.4007092. [PubMed: 22938355]

[24]. Zhang J, Gellman B, Koert A, Dasse KA, Gilbert RJ, Griffith BP, et al. Computational and experimental evaluation of the fluid dynamics and hemocompatibility of the CentriMag blood pump. Artif Organs 2006;30(3):168–77. 10.1111/j.1525-1594.2006.00203.x. [PubMed: 16480391]

[25]. Sobieski MA, Giridharan GA, Ising M, Koenig SC, Slaughter MS. Blood trauma testing of CentriMag and RotaFlow centrifugal flow devices: a pilot study. Artif Organs 2012;36(8):677–82. 10.1111/j.1525-1594.2012.01514.x. [PubMed: 22882437]

[26]. Guan Y, Su X, McCoach R, Kunselman A, El-Banayosy A, Ündar A. Mechanical performance comparison between RotaFlow and CentriMag centrifugal blood pumps in an adult ECLS model. Perfusion 2010;25(2):71–6. 10.1177/0267659110365366. [PubMed: 20212070]

[27]. Palanzo DA, El-Banayosy A, Stephenson E, Brehm C, Kunselman A, Pae WE. Comparison of hemolysis between C entri M ag and R ota F low rotary blood pumps during extracorporeal membrane oxygenation. Artif Organs 2013;37(9):E162–6. 10.1111/aor.12158. [PubMed: 23981131]

[28]. Chen Z, Jena SK, Giridharan GA, Sobieski MA, Koenig SC, Slaughter MS, et al. Shear stress and blood trauma under constant and pulse-modulated speed CF-VAD operations: CFD analysis of the HVAD. Med Biol Eng Comput 2019;57(4):807–18. 10.1007/s11517-018-1922-0. [PubMed: 30406881]

[29]. Zhang J, Zhang P, Fraser KH, Griffith BP, Wu ZJ. Comparison and experimental validation of fluid dynamic numerical models for a clinical ventricular assist device. Artif Organs 2013;37(4):380–9. 10.1111/j.1525-1594.2012.01576.x. [PubMed: 23441681]

[30]. Faghih MM, Keith Sharp M. Extending the power-law hemolysis model to complex flows. J Biomech Eng 2016;138(12). 10.1115/1.4034786.

[31]. Ding J, Niu S, Chen Z, Zhang T, Griffith BP, Wu ZJ. Shear-induced hemolysis: species differences. Artif Organs 2015;39(9):795–802. 10.1111/aor.12459. [PubMed: 25899978]

[32]. Taskin ME, Fraser KH, Zhang T, Wu C, Griffith BP, Wu ZJ. Evaluation of Eulerian and Lagrangian models for hemolysis estimation. Am Soc Artif Intern Organs J 2012;58(4):363–72. 10.1097/MAT.0b013e318254833b.

[33]. F1841-19 A. Standard Practice for Assessment of Hemolysis in Continuous Flow Blood Pumps. American Society for Testing and Materials. West Conshohocken; PA(U.S.A.).

[34]. Berk ZB, Zhang J, Chen Z, Tran D, Griffith BP, Wu ZJ. Evaluation of in vitro hemolysis and platelet activation of a newly developed maglev LVAD and two clinically used LVADs with human blood. Artif Organs 2019;43(9):870–9. 10.1111/aor.13471. [PubMed: 31001834]

[35]. Chen Z, Zhang J, Li T, Tran D, Griffith BP, Wu ZJ. The impact of shear stress on device-induced platelet hemostatic dysfunction relevant to thrombosis and bleeding in mechanically assisted circulation. Artif Organs 2020;44(5):E201–13. 10.1111/aor.13764. [PubMed: 31849074]

[36]. Gross-Hardt S, Hesselmann F, Arens J, Steinseifer U, Vercaemst L, Windisch W, et al. Low-flow assessment of current ECMO/ECCO2R rotary blood pumps and the potential effect on hemocompatibility. Crit Care 2019;23(1):1–9. 10.1186/s13054-019-2622-3. [PubMed: 30606235]

[37]. Simmonds MJ, Atac N, Baskurt OK, Meiselman HJ, Yalcin O. Erythrocyte deformability responses to intermittent and continuous subhemolytic shear stress. Biorheology 2014;51(2–3):171–85. 10.3233/BIR-140665. [PubMed: 24948378]

[38]. Horobin JT, Sabapathy S, Simmonds MJ. Red blood cell tolerance to shear stress above and below the subhemolytic threshold. Biomech Model Mechanobiol 2020;19(3):851–60. 10.1007/s10237-019-01252-z. [PubMed: 31720887]

[39]. Sohrabi S, Liu Y. A cellular model of shear-induced hemolysis. Artif Organs 2017; 41(9):E80–91. 10.1111/aor.12832. [PubMed: 28044355]

[40]. Palanzo DA, Baer LD, El-Banayosy A, Wang S, Undar A, Pae WE. Choosing a pump for extracorporeal membrane oxygenation in the USA. Artif Organs 2014;38(1):1–4. 10.1111/aor.12215. [PubMed: 24392864]

[41]. Chen Z, Mondal NK, Ding J, Gao J, Griffith BP, Wu ZJ. Shear-induced platelet receptor shedding by non-physiological high shear stress with short exposure time: glycoprotein Ibα and glycoprotein VI. Thromb Res 2015;135(4):692–8. 10.1016/j.thromres.2015.01.030. [PubMed: 25677981]

[42]. Chen Z, Mondal NK, Ding J, Koenig SC, Slaughter MS, Griffith BP, et al. Activation and shedding of platelet glycoprotein IIb/IIIa under non-physiological shear stress. Mol Cell Biochem 2015;409(1):93–101. 10.1007/s11010-015-2515-y. [PubMed: 26160282]

[43]. Han D, Zhang J, Griffith BP, Wu ZJ. Models of shear-induced platelet activation and numerical implementation with computational fluid dynamics approaches. J Biomech Eng 2022;144(4). 10.1115/1.4052460.

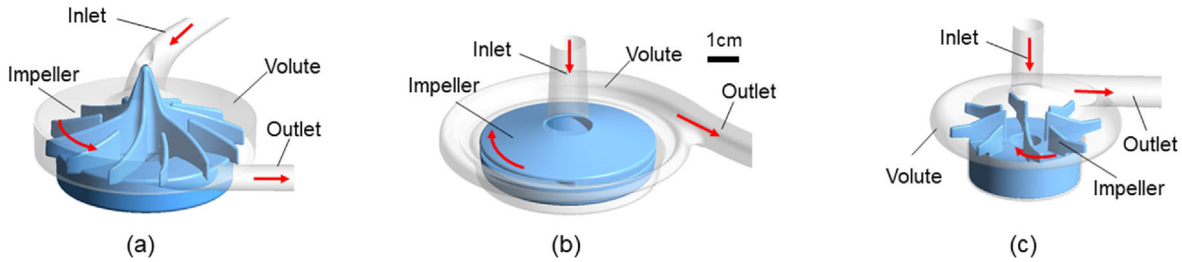

Fig. 1.

3D geometries and primary flow paths of the (a) Revolution, (b) Rotaflow and (c) CentriMag pump.

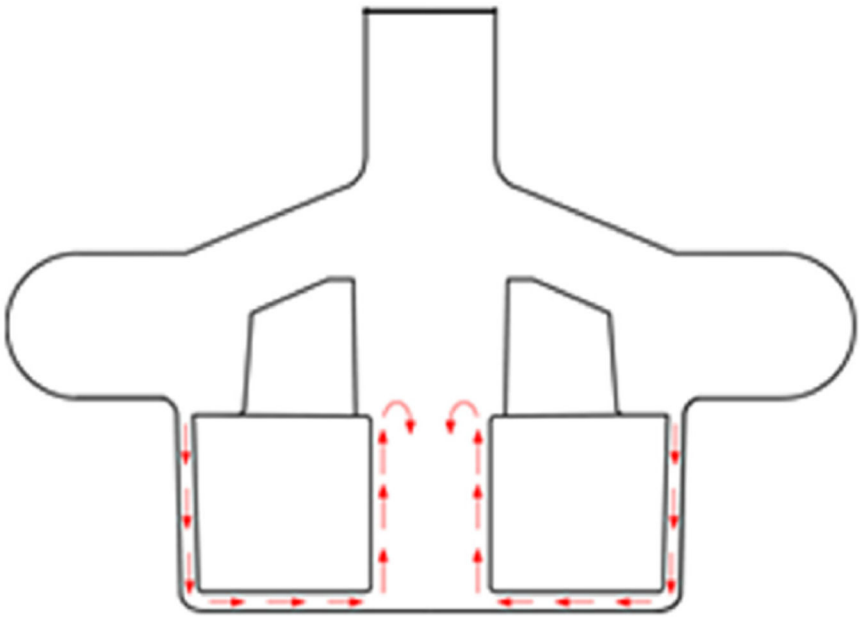

Fig. 2.
Schematical illustration of the secondary flow path in the small gaps between the impeller hub and stationary pump housing. CentriMag is used as an example.

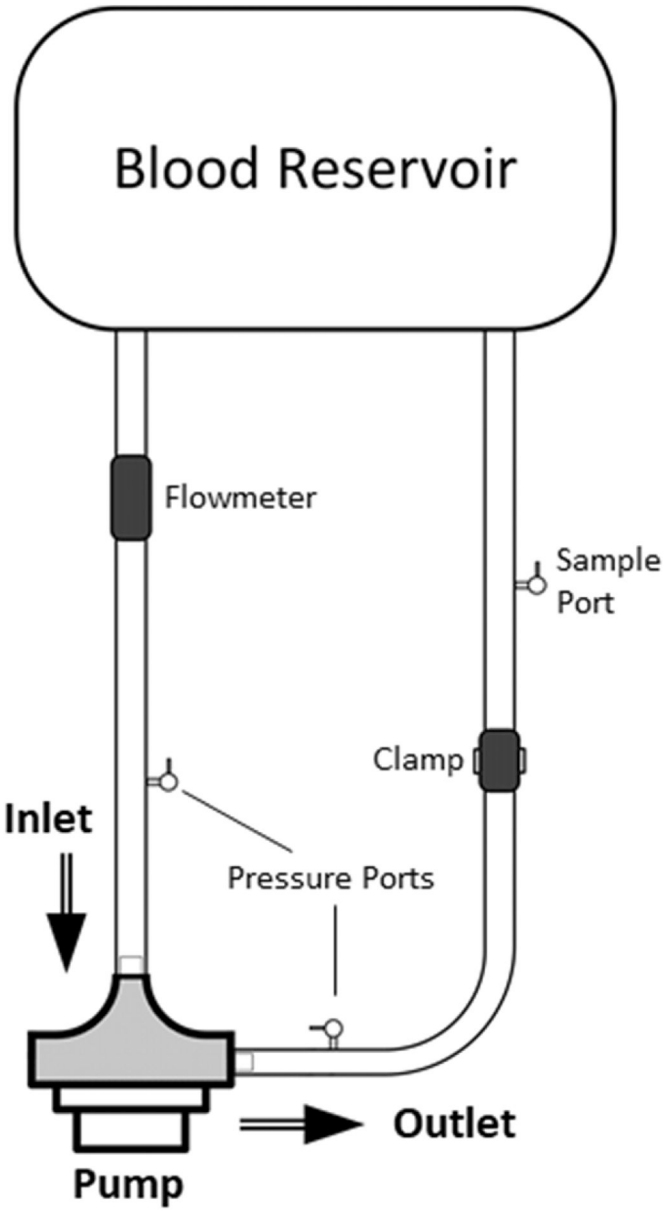

Fig. 3.
Schematical illustration of the blood circulatory loop experiment setting.

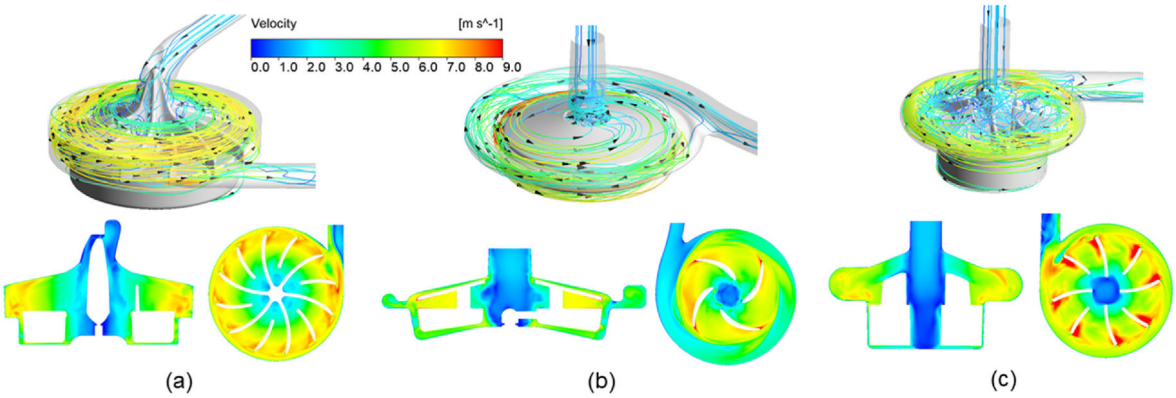

Fig. 4.

Streamlines (top row) and velocity fields (bottom row) of (a) the Revolution, (b) Rotaflow, and (c) CentriMag blood pumps under the pressure head of 350 mmHg and flow rate of 5 L/min.

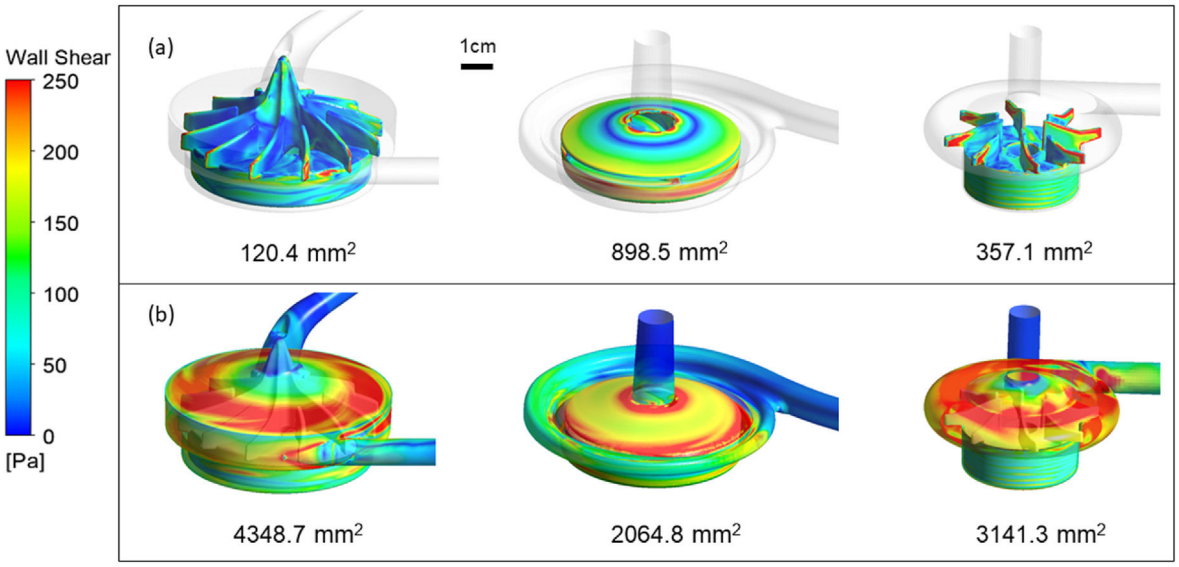

Fig. 5.

WSS distributions on the (a) impellers, and (b) housings of the Revolution (left), Rotaflow (middle) and CentriMag (right) blood pumps. The areas of the higher WSS (>200 Pa) surfaces are calculated and displayed below each pump.

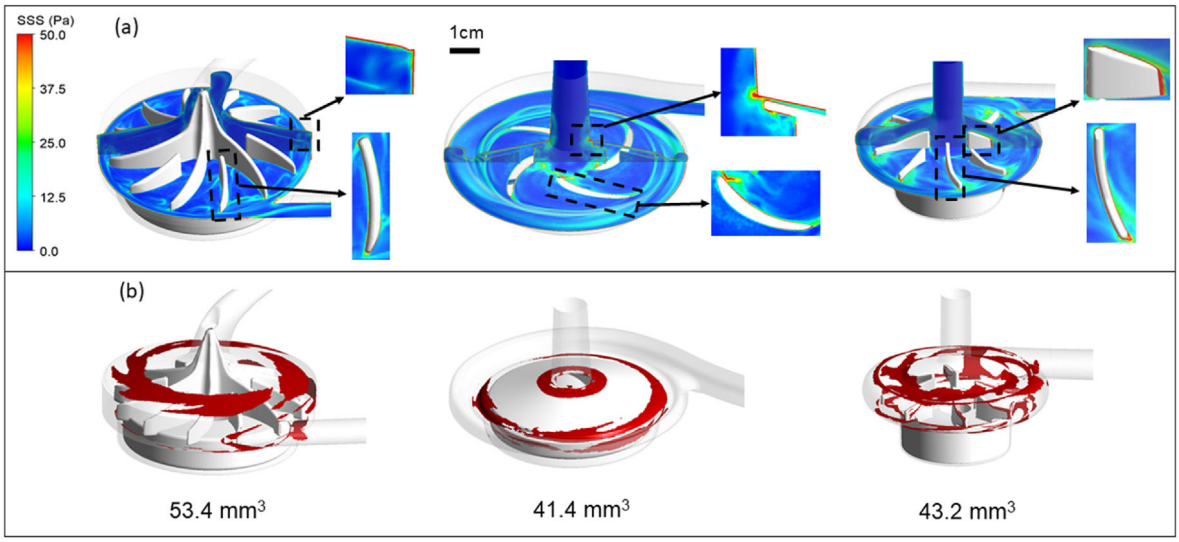

Fig. 6.

(a) SSS distributions within the Revolution (left), Rotaflow (middle) and CentriMag (right) blood pumps. (b) The volume of higher SSS (>200 Pa) regions in each pump.

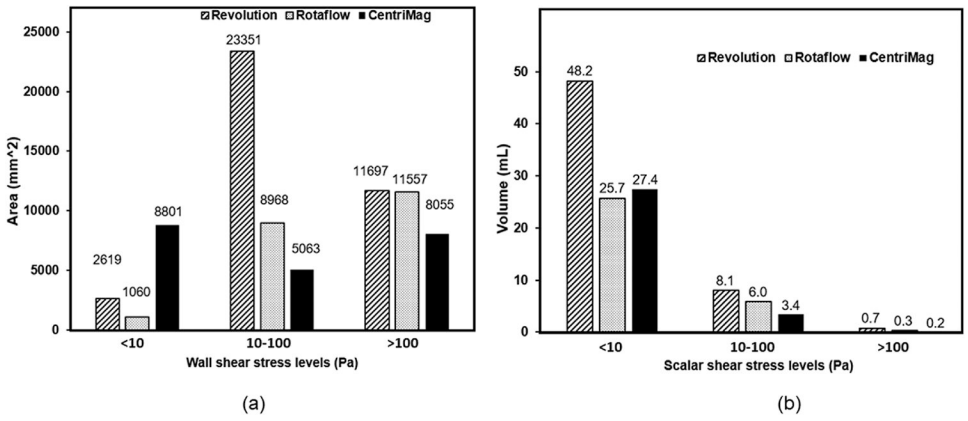

Fig. 7.

(a) WSS and (b) SSS level distributions of the Revolution, Rotaflow and CentriMag pumps running under the pressure head of 350 mmHg and flow rate of 5 L/min.

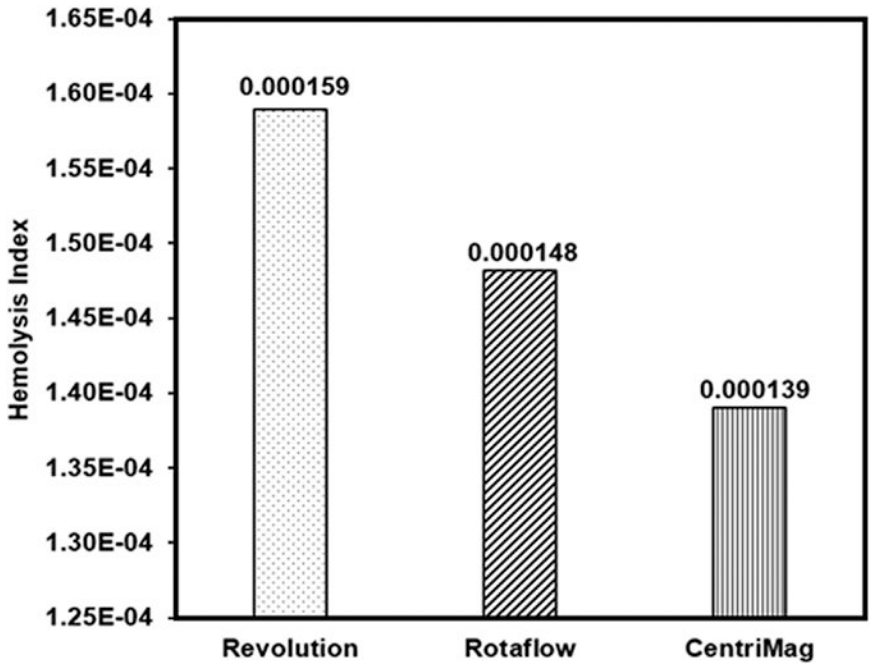

Fig. 8.

(a) CFD predicted HI of the three pumps running under the pressure head of 350 mmHg and flow rate of 5 L/min.

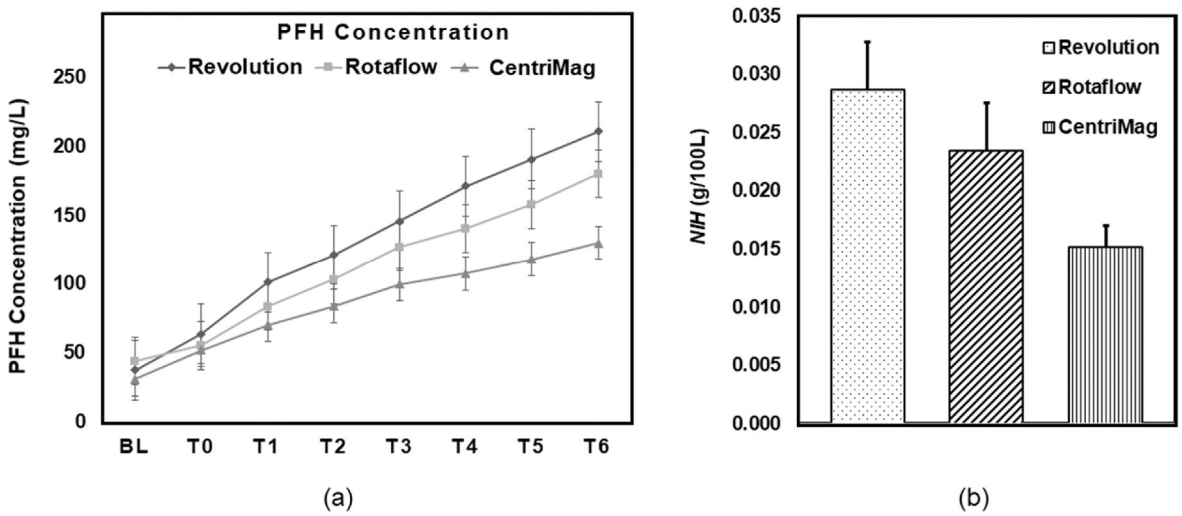

Fig. 9.

(a) PFH concentration values and (b) Experimental NIH (g/100 L) of the Revolution, Rotaflow and CentriMag blood pumps (pressure head of 350 mmHg and flow rate of 5 L/min).

Table 1

Pump characteristics.

Pump	Revolution	RotaFlow	CentriMag
Shroud	No	Yes	No
Bearing	Two pin-bearings	One ball-and-cap	Magnetic bearing
Weight (gram)	94.5	61.3	67.3
Priming volume (mL)	57	32	31
Maximum RPM	3,500	5,000	5,500
Maximum flow (L/min)	8	9.9	9.9